Sheffield Hallam University

Cathodic protection of steel framed masonry structures - experimental and numerical studies

LAMBERT, Paul <http://orcid.org/0000-0002-2815-1674>, MANGAT, Pal <http://orcid.org/0000-0003-1736-8891>, O'FLAHERTY, Fin <http://orcid.org/0000-0003-3121-0492> and WU, You-Yo

Available from Sheffield Hallam University Research Archive (SHURA) at:

https://shura.shu.ac.uk/3049/

This document is the Accepted Version [AM]

Citation:

LAMBERT, Paul, MANGAT, Pal, O'FLAHERTY, Fin and WU, You-Yo (2008). Cathodic protection of steel framed masonry structures - experimental and numerical studies. Materials and structures, 41 (2), 301-310. [Article]

Copyright and re-use policy

See http://shura.shu.ac.uk/information.html

Sheffield Hallam University Research Archive
http://shura.shu.ac.uk

Sheffield Hallam University, Howard Street, Sheffield, S1 1WB, United Kingdom.
Tel: +44 (0) 114 225 3525. Fax: +44 (0) 114 225 4546. E-Mail: p.lambert@shu.ac.uk

Cathodic Protection of Steel Framed Masonry Structures - Experimental and Numerical Studies

P Lambert, P S Mangat & F J O'Flaherty
Centre for Infrastructure Management, Sheffield Hallam University, United Kingdom

Y-Y Wu
Scott Wilson, Royal Court, Basil Close, Chesterfield, United Kingdom

Abstract

Many high-profile steel-framed masonry buildings are susceptible to extensive damage as a result of corrosion of the steel frame. This has resulted in serious consequences with respect to serviceability, safety, aesthetics and heritage. Cathodic protection (CP) is a proven method for preventing and protecting buried and submerged steel and reinforced concrete structures from corrosion. More recently, the method has been introduced to prevent and control corrosion in steel-framed masonry structures. However, despite several sizeable CP installations around the world, there are no formal guidelines for the design, installation and operation of such systems and much of the knowledge is based on empirical observations. This paper presents both experimental and numerical studies on the cathodic protection of representative steel framed masonry structures. These studies are considered essential in the understanding of the mechanisms of cathodic protection and the design of optimised cathodic protection systems for such structures.

Keywords: corrosion, steel frame, cathodic protection, impressed current, numerical modelling.

INTRODUCTION

The identification of "Regent Street Disease" in the United Kingdom in the late 1970's first highlighted the problems of the corrosion of iron and steel frames and other structural components occurring on a significant number of the grand and often listed structures in many city centres [1]. This

form of steel-framed construction initially employed in Chicago and subsequently used in most US and European cities in the first two decades of the 20th century, has resulted in problems with respect to serviceability, safety, aesthetics and heritage. Cathodic protection, originally developed by Humphry Davy [3] and later employed widely on buried and submerged structures, was first considered for reinforced concrete in the late 1950's [4]. It was not until the development of improved anode systems based on catalysed titanium and titanium oxide in the early 1980's [5] and the considerable advances in digital operating systems that it became a viable commercial solution for corrosion prevention. The transfer of CP to steel-framed buildings was somewhat slower and it was not until 1997 that the first full structure was protected by electrochemical means [1]. Despite several sizeable installations there are no formal guidelines for the design, installation and operation of such systems and much of the knowledge is based on empirical observations [6].

Specific design standards for cathodic protection of steel-framed structures currently do not exist [2]. The existing standards such as NACE (2000), "Standard RP0290-2000, Impressed Current Cathodic Protection of Reinforcing Steel in Atmospherically Exposed Concrete Structures" [7] and European Standards (2000), "EN 12696:2000, Cathodic Protection of Steel in Concrete" [8] are not specific for steel-framed masonry structures and are not directly applicable. In the absence of formal design guidelines and standards specifically for the cathodic protection of steel-framed masonry structures, it has become common practice for pilot schemes or trial installations to be employed in determining the suitability and design of CP systems for such applications.

The finite element method and boundary element method have been used to analyse the protective current and potential distribution of cathodically protected reinforced concrete structures [9] and offshore or marine structures [10-13] respectively. More recently, the latter has been introduced to analyse cathodic protection systems for steel-framed masonry structures [6], which is developed in this paper. One of the major problems in understanding the mechanisms of cathodic protection in steel-framed construction is the relatively complex geometry of the systems under consideration. No

information exists about current throw onto typical steel sections, yet this is fundamental to the design of CP systems.

This paper presents both experimental and numerical studies on the distribution of protective current and potential in representative cathodic protection systems for steel-framed masonry structures whereby sand is employed to represent the masonry encasement. It is expected that the output from this work, together with other studies to be published by the authors using masonry rather than sand, will progress the development of this technology and contribute to the development of the formal guidelines and standards for cathodic protection of steel framed masonry structures.

EXPERIMENTAL PROCEDURE

Model Impressed Current Cathodic Protection System

The principle and basic components of impressed current cathodic protection systems (ICCP) have been well described [14]. Based on these, two ICCP systems for steel-framed masonry structures have been constructed for analyzing the distribution of the protective potential and current. The main components of the systems employed in this study are a manual power supply; discrete anodes based on a titanium oxide ceramic; steel 'I' section specimens employed as the cathodes (see Figures 1 & 2) and sandboxes fabricated from uPVC, 1 m square by 0.25 m in depth. Building sand was employed to represent the masonry and was tamped in layers to ensure good compaction. The moisture content of the sand was adjusted to achieve a resistivity within the range 10 to 50 kΩ.cm representing the range commonly encountered in brick and stone masonry. Dependent upon the type of steel section, two ICCP systems were constructed. For System A, where the cathode is steel section A representing a stanchion, the test facility and its components are shown in Figures 3 and 4. System B, for which steel section B was used as the cathode, was similar in set-up to System A but was buried horizontally to represent a beam, as shown in Figure 5.

Each system was connected to a power supply and monitoring equipment and energised. There are two common methods of controlling ICCP systems. One is to keep the output voltage constant and allow

the current to alter in order to maintain the set potential. The other method is to fix the current and allow the potential to float. In this work, the former approach of fixed potential was employed. Once the output current became stable, the distribution of protective potential was measured by means of a standard copper/copper sulphate reference electrode suitable for use in direct contact with sand.

Measurements of Protective Potential

The potential distribution on a grid of sandbox free surface was measured under a range of test conditions, including the various anode coordinates, sand resistivities and output currents, by moving a hand-held copper/copper sulphate reference electrode over the surface. It should be noted that such measured potentials do not represent the actual protective potential values on the surface of the steel section. They incorporate a potential drop or IR_{Ω}. In order to obtain the value of the IR_{Ω}-free CP protective potential on the surface of steel, the instant-off potential method is employed, whereby the current is briefly interrupted (turned off) and a value of potential taken immediately afterwards whilst no current is flowing and there is, therefore, no potential drop. The power is then reapplied. As the steel section has a very complex geometry, it is not possible to accurately measure every point on the steel surface. Due to this limitation, only the protective potential at selected points on the top surface of the steel section was measured.

BOUNDARY ELEMENT METHOD

For a uniform isotropic electrolyte, the flow of current can be shown to obey the following Laplace equation, as represented in Figure 6 [10 - 13]:

$$k\nabla^2 E(p) = 0 \qquad p \in \Omega \tag{1}$$

Where E is the potential at any p (x, y, z) of domain

k is the conductivity of electrolyte

Ω is the problem domain

The problem in cathodic protection is to solve the above Laplace equation subject to the following boundary conditions:

$$E = E_0 \qquad \text{on } \Gamma_1 \tag{2}$$

$$i = k\frac{\partial E}{\partial n} = i_0 \qquad \text{on } \Gamma_2 \tag{3}$$

$$i_a = -f_a(E_a) \qquad \text{on } \Gamma_a \tag{4}$$

$$i_c = -f_c(E_a) \qquad \text{on } \Gamma_c \tag{5}$$

where $\Gamma(=\Gamma_1+\Gamma_2+\Gamma_a+\Gamma_c)$ is the surface of the electrolyte domain Ω, E_0 and i_0 are the prescribed values of potential and current density respectively. Equations (4) and (5) describe the relationship between the potential E and current density i on the anode surface and cathode surface separately, known as the polarisation curves, and are experimentally determined. A series of linear algebraic equations are generated which may be written in matrix notation [15,16]:

$$\boldsymbol{HE=Gi} \tag{6}$$

where $\boldsymbol{H}$ and $\boldsymbol{G}$ are the (n x n) square matrices, called the influence matrices, and $\boldsymbol{E}$ and $\boldsymbol{i}$ contains the nodal potential vectors and the nodal normal current density vectors separately. Rearranging equation (6) to get all known values on the right-hand side and then multiplying out, and all unknown values on the left-hand side, gives:

$$\boldsymbol{AX=F} \tag{7}$$

where $\boldsymbol{A}$ is the coefficient matrix, $\boldsymbol{X}$ is the vector of the unknown values of potential and current density on the boundaries, and $\boldsymbol{F}$ is an independent vector. For the linear boundary conditions, the above equation can be solved by Gauss Elimination or LU Decomposition. However, in practice the boundary conditions on the anodes and cathodes are represented by the non-linear polarisation curves. Equation (7) is, therefore, solved by an interactive procedure [12,17]. After all values of the potential

and current densities in equation (7) are solved, the solutions of the internal point in electrolyte domain can be calculated [15,16].

RESULTS and DISCUSSION

Boundary Element Analysis of ICCP System A (stanchion)

The potential and current density distributions of ICCP System A (stanchion) have been analyzed under the conditions shown in Table 1.

Table 1: Test Conditions, ICCP System A (stanchion)

ICCP System A		**Case 1**	**Case 2**	**Case 3**	**Case 4**
Average Sand Resistivity (kΩ.cm)		42.3	14.6	14.6	14.6
Anode Co-ordinates	**P1**	X = 50.0 cm Y = 30.0 cm Z = 6.0 cm	X = 50.0 cm Y = 30.0 cm Z = 6.0 cm	X = 50.0 cm Y = 15.0 cm Z = 6.0 cm	X = 35.0 cm Y = 52.8 cm Z = 6.0 cm
	P2	X = 50.0 cm Y = 30.0 cm Z = 16.0 cm	X = 50.0 cm Y = 30.0 cm Z = 16.0 cm	X = 50.0 cm Y = 15.0 cm Z = 16.0 cm	X = 35.0 cm Y = 52.8 cm Z = 16.0 cm
Applied Current Density (mA/cm^2)		7.95			

The purpose of Cases 1 and 2 was to investigate the effect of resistivity on the distribution of protective potential and current density under the same anode locations and a given anode current density. Upon completion of these cases the anode is moved to the locations for Cases 3 and 4 for further analysis in order to study the effect of the anode locations on the distributions of protective potential and current density. The total boundary element mesh used for the analysis is shown in Figures 7 and 8. Examples of the modelling results are shown Figures 9 to 11.

Boundary Element Analysis of ICCP System B (beam)

The potential and current density distributions of ICCP System B were analyzed under the conditions shown in Table 2. Again, the purpose of Cases 1 and 2 was to investigate the effect of the resistivity on the distributions of protective potential and current density under the same anode locations and a given anode current density . On completion of these cases the anodes were moved to the locations shown for Case 3 for further analysis in order to study the effect of the anode locations on the distributions of protective potential and current density. The total boundary element mesh used for the

analysis is shown in Figures 12 and 13 and examples of the modelling results are shown Figures 14 to 16.

Table 2: Test Conditions, ICCP System B (beam)

ICCP System B			**Case 1**	**Case 2**	**Case 3**
Average Sand Resistivity (kΩ.cm)			42.3	14.6	14.6
Anode Co-ordinates	**Anode A**	**P1**	X = 36.2 cm Y = 10.0 cm Z = 6.0 cm	X = 36.2 cm Y = 10.0 cm Z = 6.0 cm	X = 21.2 cm Y = 10.0 cm Z = 6.0 cm
		P2	X = 36.2 cm Y = 10.0 cm Z = 16.0 cm	X = 36.2 cm Y = 10.0 cm Z = 16.0 cm	X = 21.2 cm Y = 10.0 cm Z = 16.0 cm
	Anode B	**P1**	X = 63.8 cm Y = 90.0 cm Z = 6.0 cm	X = 63.8 cm Y = 90.0 cm Z = 6.0 cm	X = 78.8 cm Y = 90.0 cm Z = 6.0 cm
		P2	X = 63.8 cm Y = 90.0 cm Z = 16.0 cm	X = 63.8 cm Y = 90.0 cm Z = 16.0 cm	X = 78.8 cm Y = 90.0 cm Z = 16.0 cm
Applied Current Density (mA/cm^2)			1.6		

Discussion

The modelling results on ICCP Systems A and B both show that there is a significant variation of protective potential and current density in different regions of the steel surface. This variation is related to the resistivity of the sand, the anode locations and the geometry of the steel section.

Under the conditions of the same applied current density and anode locations, the results in Cases 1 and 2 of both ICCP Systems A and B demonstrate that a higher electrolyte resistivity results in a less uniform protective potential (Figures 10 and 15) while the distribution of the protective potential and current is more uniform in a lower resistivity electrolyte. A higher resistivity electrolyte also results in a lower protective current density on the surface of steel.

The anode locations have a significant influence on the potential and current distribution on the steel surface (Figures 9, 11 and 14). Furthermore, it can be seen that the potential and current density distribution along the surface of steel is more uniform as the anode distance increases (Figure 16). This confirms the importance of the correct positioning of the anodes in a steel frame ICCP system in achieving the optimum level of protection over the entire structure.

The potential values calculated by the boundary element modelling on the free surface of the sandbox in Case 2 of both ICCP System A and B have been compared with experimental measurements. For clarity, only values from representative points have been reported as shown in Figures 17 and 18. It can be seen that there is good agreement between the experimental and calculated values by the boundary element method. However, there are small differences between them due to one or more of the following reasons:

i) For the boundary element modelling the sand resistivity has been assumed to be uniform, having a constant value. In reality, the sand resistivity will not remain the same and there will be some variation between different areas of the sandbox.

ii) The relationship between applied current and surface potential has been based on experimental observation and is an important factor in the determination of the boundary condition. Any variation or error in the polarisation characteristics would have a significant effect on the modelling results.

iii) It is possible that formation of a passive film on the cathodically protected steel surface has altered its characteristics.

The results demonstrate that the boundary element method provides sufficiently accurate results to make it an effective tool for the modelling and design of such systems.

CONCLUSIONS

The following conclusions are given by the experimental and numerical studies representing the cathodic protection of steel framed masonry structures reported in this paper:

1. There is a significant variation of protective potential and current density in different regions of the steel surface. This variation is related not only to the resistivity of sand and the anode locations but also to the geometry of the steel section.

2. The distribution of CP potential and current density is directly related to the resistivity of electrolyte. Under the same applied current density and anode location, the distribution of the protective potential and current density is more uniform in a low resistivity electrolyte. A higher resistivity electrolyte results in a lower protective current density on the surface of steel.

3. The anode position has a significant effect on the distribution of CP potential and current density. The potential and current density distributions along the surface of steel section becomes more uniform as the anode distance from the steel increases.

4. Boundary element modelling shows significant promise as a practical tool for designing, analysing and optimising cathodic protection system for steel framed masonry structures.

ACKNOWLEDGEMENTS

The authors would like to gratefully acknowledge the financial support of The Royal Society, Mott MacDonald Group Ltd and Sheffield Hallam University.

REFERENCES

1. Atkins C P, Lambert P and Coull, Z L (2002) Cathodic protection of steel framed heritage structures. Proc. of 9th Int. Conf. on Durability of Building Materials and Components, Australia, 11pp.
2. Wu Y-Y (2005) Cathodic protection of steel framed masonry structures. PhD Thesis, Sheffield Hallam University, UK.
3. Davy H (1825) On the corrosion of copper sheeting by seawater, and on methods of preventing this effect, and on their application to ships of war and other ships. Proceedings of the Royal Society, 114, pp.151-246, 1824 and 115, pp.328-346.
4. Heuze B (1965) Cathodic protection of steel in prestressed concrete. Materials Performance, **11**, pp.57-62.

5. Stratfull R F (1974) Experimental cathodic protection of a bridge deck, Transportation Research Record 500, Transportation Research Board, Washington DC, USA.
6. Lambert P & Wu Y-Y (2005) Electrochemical methods for the preservation of masonry clad structural frames, Maritime Heritage and Modern Ports, Proceedings of the Second International Conference on Maritime Heritage, Barcelona, pp 219-228.
7. NACE Standard RP 0290-2000 (2000) Impressed current cathodic protection of reinforcing steel in atmospherically exposed concrete structures.
8. European Standard EN 12696:2000 (2000) Cathodic protection of steel in concrete.
9. Hassanein A M, Glass G K & Buenfeld N R (2002) Potential current distribution in reinforced concrete cathodic protection systems, Cement and Concrete Composites, 24, pp.159-167.
10. Gartland P O & Johnsen R (1985) COMCAPS-Computer modelling of cathodic protection systems, NACE Corrosion ’85. Paper 319.
11. Adey R A, Niku S M, Brebbia C A & Finnegan J (1985) Computer aided design of cathodic protection, Boundary Element Methods VII, Villa Olmo, Lake Como, Italy.
12. Zamani N G (1986) Boundary element simulation of cathodic protection system in prototype ship, Applied Mathematics and Computation. **26**, (2), pp.118-134.
13. Adey R A & Niku S M (1992) Computational modelling of corrosion using boundary element methods, Computer Modelling In Corrosion, STP 1154, ASTM, Philadephia, USA, pp.248-263.
14. Broomfield J P (1997) Corrosion of steel in concrete: understanding, investigation and repair, E & FN Spon, London.
15. Brebbia C A (1978) The boundary element method for engineers, Pentech Press, London.
16. Brebbia C A & Dominguez J (1989) The boundary elements - an introductory course, McGraw-Hill, New York.
17. Press W H (1992) Numerical recipe in Fortran: the art of scientific computing. Cambridge University Press.

LIST OF FIGURES

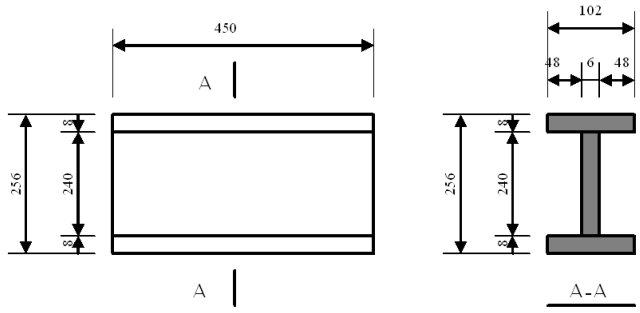

Figure 1: Steel Section A (unit: mm - not to scale)

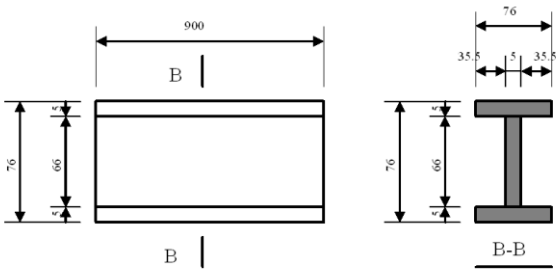

Figure 2: Steel Section B (unit: mm - not to scale)

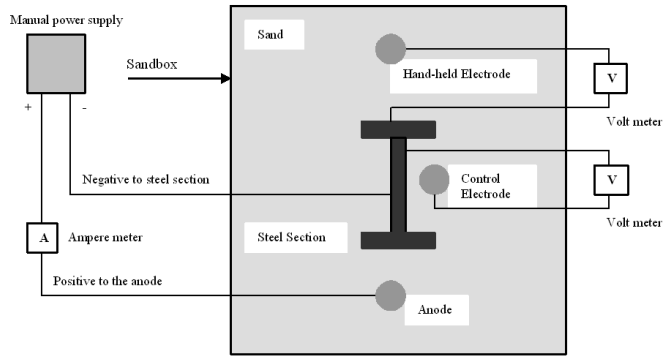

Figure 3: Schematic illustration of test facility (ICCP System A)

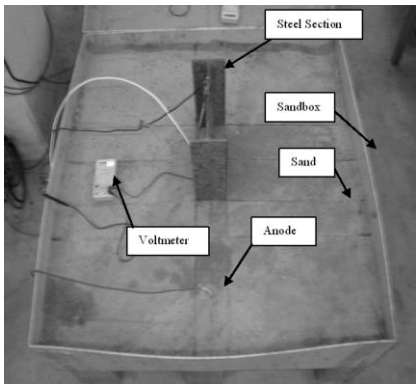

Figure 4: Components of ICCP System A

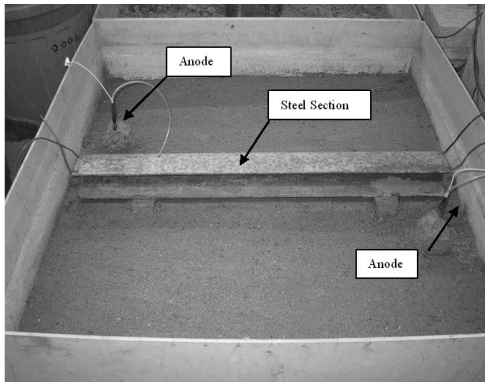

Figure 5: Buried steel section B and two anodes, shown with the sand removed

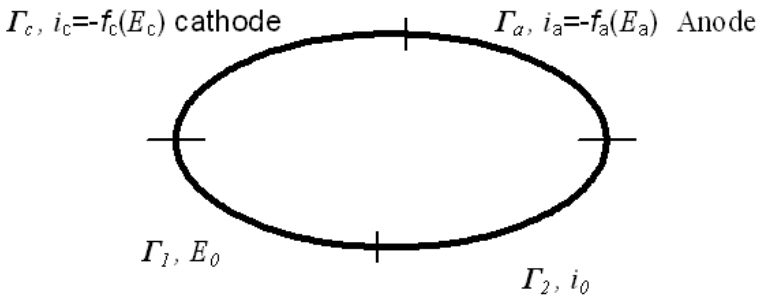

Figure 6: Basic equations and boundary conditions for a uniform isotropic electrolyte

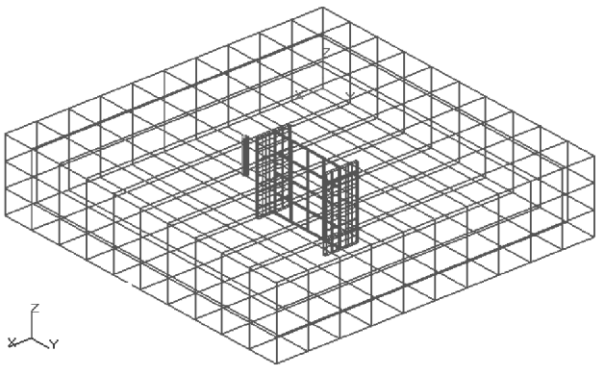
Figure 7: Schematic representation of the total boundary element mesh for ICCP System

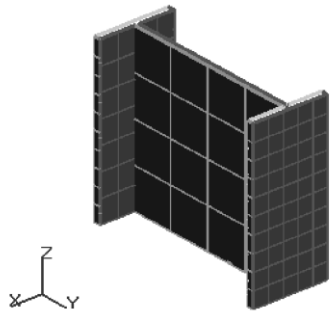

Figure 8: Schematic representation of the boundary element mesh on the surface of Steel Section A of ICCP System A

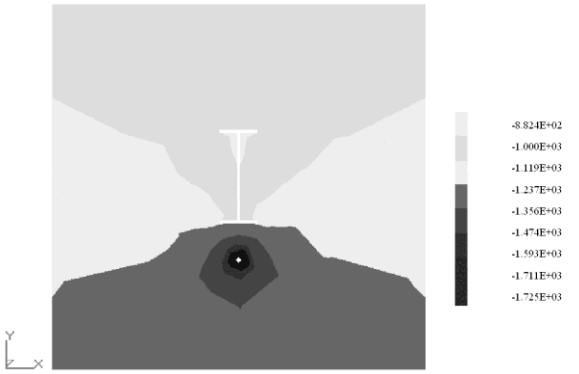

Figure 9: Potential distribution at Z=11.0cm of ICCP System A (mV, vs CSE, Case 1)

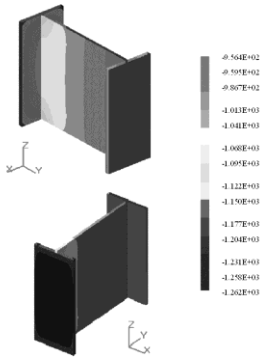

Figure 10: Potential distribution on the surface of Steel Section A of ICCP System A (mV, vs CSE, Case 1)

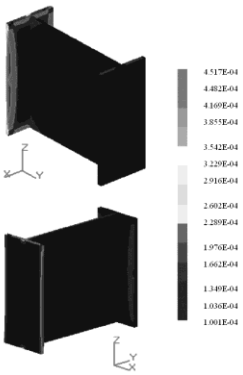

Figure 11: Current distribution on the surface of Steel Section A of ICCP System A (mA, Case 3)

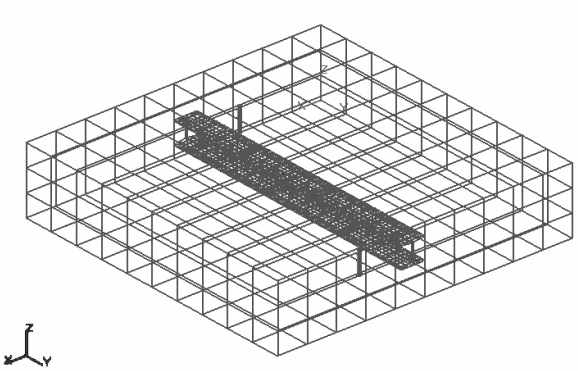

Figure 12: Schematic representation of the total boundary element mesh for ICCP System B

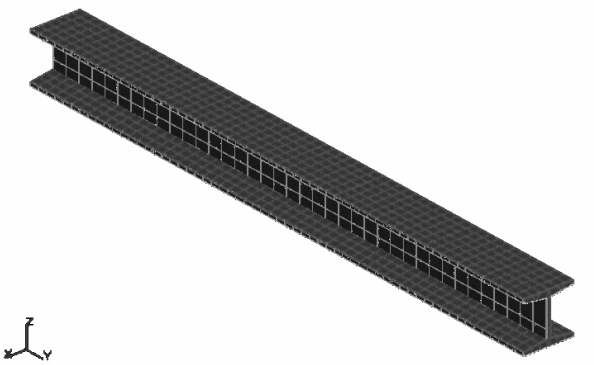

Figure 13: Schematic representation of the boundary element mesh on the surface of Steel Section B of ICCP System B

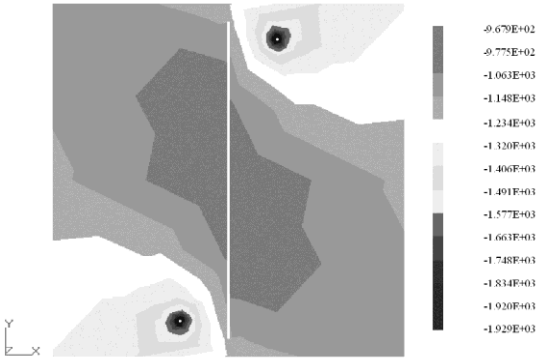

Figure 14: Potential distribution at Z=11.0cm of ICCP System B (mV, vs CSE, Case 1)

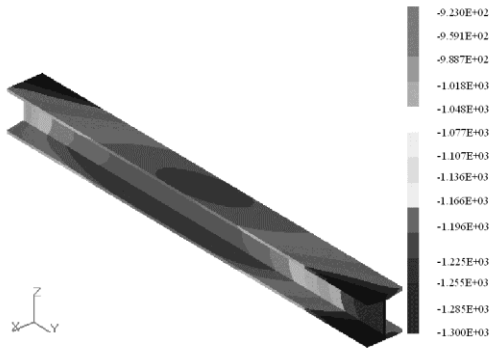

Figure 15: Potential distribution on the surface of Steel Section B of ICCP System B (mV, vs CSE, Case 1)

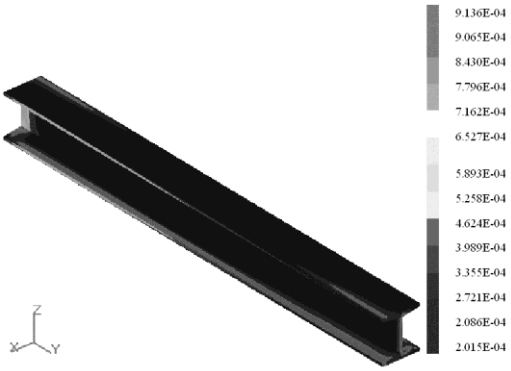

Figure 16: Current distribution on the surface of Steel Section B, ICCP System B (mA, Case 3)

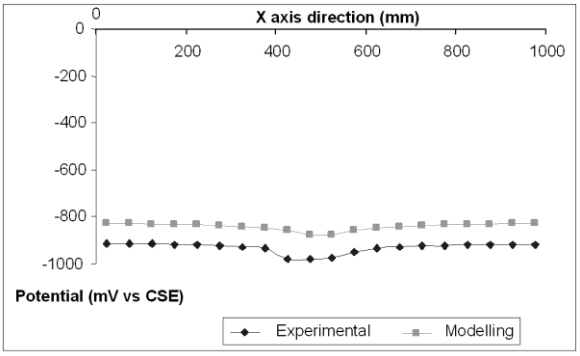

Figure 17: Case 2, ICCP System A: Comparison of experimental potential with boundary element solutions at grid reference Y=27.50cm, Z=22.00cm on the surface of the sandbox.

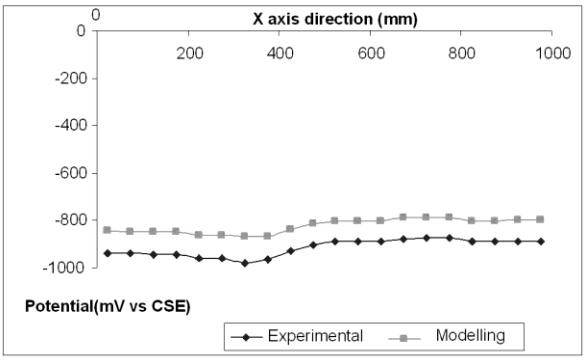

Figure 18: Case 2, ICCP System B: Comparison of experimental potential with boundary element solutions at grid reference Y=12.50cm, Z=22.00cm on the surface of the sandbox.